

# Experimental Study on the Thermodynamic Damage Power of Ammunition Deflagration in a Closed Explosive Device

Liangquan Wang,\* Fei Shang and Deren Kong

*School of Mechanical Engineering, Nanjing University of Science and Technology, Jiangsu - 210 094, China*

*\*E-mai:wlq2223263181@163.com*

## ABSTRACT

The high temperature and high pressure gas produced by propellant deburning has strong thermal effect, which will produce strong thermal damage effect on the target. In this study, an improved closed explosive device was used to simulate the thermal shock loading of 5/7 single base propellant with a charge mass of 17.4 g, and the change law of heat flow density of propellant in the process of deflagration in a closed environment was tested. The experimental results show that the temperature rises rapidly during the deflagration of the 5/7 single-base propellant, and the maximum heat flow density can reach 17.68 MW/m<sup>2</sup>. The curves obtained from the three tests have good consistency in the change trend, which proves the engineering practicability of the improved closed explosive device in the study.

**Keywords:** Closed explosives device; Propellants; Heat flow density; Thermal shock loading

## 1. INTRODUCTION

Propellant has fast combustion speed, high pressure, stable performance and good stability, it is an indispensable energy source for the launch of weapons and equipment such as guns, shells, grenades, rockets, missiles, and mines.<sup>1-3</sup> After the propellant is detonated, it expands rapidly to generate a large amount of high-temperature and high-pressure gas to push the projectile forward at high speed, giving the projectile a certain firing speed. The projectile initial velocity directly determines the projectile damage effect on the target in the hitting target process.<sup>4-6</sup> Therefore, clarifying the projectile propellant characteristics has a very important role in evaluating the ammunition damage power and guiding ammunition design.

At present, the analysis of combustion and interior ballistic performance characteristics of propellants is an active field of research carried out by scholars all over the world and has achieved some fruitful research results. For example, in order to estimate the propellant charge internal ballistic performance, Zhao,<sup>7</sup> Y.H., *et al.* established a method to detect the static combustion performance parameters of the propellant based on the closed explosive test and predict the internal ballistic performance of the propellant. Using different batches of single-zhang-5/7 propellant, the prediction calculation of charging performance was carried out. The test results show that the established method for predicting the propellant charge internal ballistic performance based on the closed explosive test has high accuracy, it can effectively and accurately predict the internal ballistic performance of propellant samples different batches. In order to describe the output performance of Al/

KClO<sub>4</sub> igniter more accurately, Liang, X.A. *et al.*<sup>8</sup> introduced the gunpowder force correction coefficient, they established an improved Al/KClO<sub>4</sub> internal ballistic analysis model. Combined with the experimental analysis, it is shown that the pressure peak generated by the Al/KClO<sub>4</sub> igniter increases with the increase of the dosage and decreases with the increase of the cavity volume.

Ren, W.Y. *et al.*<sup>9</sup> took the airtight explosive device as the research object, calculated the characteristic quantities of two different charging methods of 18/1 and 11/7 with the same structure, obtained the pressure change law of the constant volume under ideal conditions, and calculated the gunpowder at the same time. The shape function  $\psi$ -z curve of the ballistic characteristic quantity, and the calculation results provide a reference for the study of the gunpowder combustion law and the charge safety. Wang,<sup>10</sup> X.Q. *et al.* found that an ideal propellant should have a special combustion intensity distribution by comparing and analyzing the dynamic combustion in the closed explosive propellant chamber and the static combustion process. By analyzing the difference between the ideal propellant and the actual propellant's burning intensity distribution, a quantitative evaluation method for the propellant static combustion based on the closed explosive test is proposed, and the evaluation results are in good agreement with the dynamic test results.

To study the influence of pressure wave during propellant combustion on interior ballistic performance, Jiang,<sup>11</sup> D.D., *et al.* obtained through numerical simulation that Taylor cavity surface will appear wrinkles during propellant combustion, resulting in poor interior ballistic stability and increased pressure oscillation. In order to study the interior ballistic characteristics of propellant mortars, Sun,<sup>12</sup> M.L. and others simulated the

reaction flow field in the interior ballistic process, analysed the coupling relationship between the complex gas flow field and propellant combustion, and the formation mechanism of pressure oscillation. It is obtained that the concentrated combustion of propellant caused by reflective waveguide makes the pressure behave as an oscillatory development process. Xiong,<sup>13</sup> J.M. *et al.* predicted the impact of propellant particle breakage on the interior ballistic performance of the countersunk projectile gun based on the special charge structure and secondary ignition program of the countersunk projectile. The numerical simulation results show that the more the propellant is broken, the more the maximum chamber pressure and muzzle velocity of the projectile increase, and the more intense the change in the chamber.

The high-temperature and high-pressure gas generated by the propellant deflagration not only has a high driving pressure, but also has a strong thermal effect, which will cause strong thermal shock, ablation, and even thermal damage to the target object. However, the thermal shock properties have not been studied in depth. In this study, the thermal effect of propellant deflagration in a closed explosive device is studied. The structure of the existing closed explosive device was improved, and the deflagration test of 17.4g 5/7 single base propellant was carried out. The 5/7 single-base propellant is selected because it has the characteristics of uniform mass of propellant column, good combustion performance, high energy density and good reproducibility of performance parameters, which is very suitable for experimental research. A self-developed heat flux sensor was installed on the closed explosive device to obtain the thermal shock curve during the deignition process of the propellant, and the thermal shock characteristics during the deignition process were analyzed, so as to provide scientific data support for the evaluation of the thermal shock damage power in the closed environment of the propellant and the subsequent design of the propellant.

## 2. CLOSED EXPLOSIVE DEVICE SIMULATED THERMAL SHOCK TEST SYSTEM

### 2.1 Composition of the Test System

The test system is mainly composed of a closed explosive device, a heat flux density sensor, a shock wave pressure sensor, a signal conditioner and a data acquisition system. The system block diagram is shown in Fig. 1.

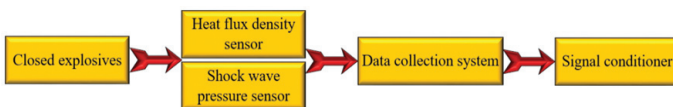


Figure 1. Test system composition block diagram.

In the above measuring system, the shock wave pressure sensor is selected 113B piezoelectric pressure sensor produced by PCB company in the United States. The signal conditioning device was developed by Nanjing University of Science and Technology, and the data collector was TranNET 308S produced by Elsys of Switzerland. The detailed technical indexes and parameters of each instrument in the test system are shown in the following Table 1.

Table 1. Detailed technical parameters of the instrument

113B piezoelectric pressure sensor	
Linearity	±1% FSO
Resonant frequency	≥500kHz
Sensor resolution	0.001psi
Output signal	ICP amplification output
Self developed signal conditioner	
Input signal range	0~1V
Magnification	1、10、100、200、
Low pass filter cut-off frequency	1K、5K、10K、15K、50K、
Output signal range	0~±10V
TranNET 308S data collector	
Input mode	ICP、DC、AC
Input range	±50mV~±50V
Maximum sampling rate	10MS/s
Sensor resolution	14bits
Working bandwidth	≥4MHz

During the test, a propellant was installed in the closed explosive chamber. This test used a 5/7 single-base propellant with a mass of 17.4 g. The charge aspect ratio is 2:1, and the charge shape is a cylinder. The main component of the propellant is nitrocellulose (nitrocellulose, NC), which is the main energy donor of the propellant. It can be used as a reinforcement agent in the propellant to improve the mechanical properties of the propellant. Then the heat flux density sensor was installed on the bracket and fixed, so that the sensitive element was facing seal the diversion hole of the explosive device, and it is about 1cm away from the diversion hole, and connect the sensor to the signal conditioner and data acquisition system. In order to ensure the test personnel safety, all test participants must leave the laboratory to ensure that there is no one around the test device, and then electrify and ignite the propellant.

### 2.2 Improved Design of Closed Explosive Device

The closed explosive device is a test system to study the pressure change rule of the gunpowder when it burns under the constant volume condition. In the gunpowder static analysis, the test technology of closed explosive device plays a very important role.<sup>14-15</sup>

The closed explosive device consists of a body, a compression bolt (high strength carbon structural steel 4340), a pressure relief bolt (304 stainless steel), and a pressure-controlled diaphragm ignition bolt (304 stainless steel). Its body is a circular cylindrical structure made of gun steel. The inner surfaces of the openings at both ends are threaded, and the ignition bolt is screwed in and positioned at one end, and the ignition bolt relies on the current to ignite the gunpowder, thereby igniting the gunpowder; the other end is equipped with a pressure relief bolt and a compression bolt. To maintain a certain pressure value at the initial combustion stage of the

propellant in the confined space, so as to maintain a higher burning speed of the propellant, a pressure control film is added between the pressure relief bolt and the compression bolt. The diaphragm thickness is calculated to reach a certain pressure and the diaphragm ruptures. The hot combustion products are released from the guide hole through the guide tube. The heat flux density sensor is placed under the guide hole, and the sensitive surface is facing the guide hole.

The conventional closed explosive device is directly provided with a diversion hole on the end face of the diversion pipe. When the pressure control film breaks, the debris will directly hit the sensitive surface of the sensor, causing the sensor to be directly damaged and unable to continue to measure. In order to prevent the pressure control film fragment from damaging the sensor, the opening direction of the guide hole is perpendicular to the installation direction of the pressure control film fragment, which greatly reduces the probability of the pressure control film fragment hitting the sensor, improves the survival rate of the sensor, thus improving the ability of each test sensor to obtain data, and reducing the cost of the test. The schematic diagram of the closed explosive device is shown in Fig. 2.

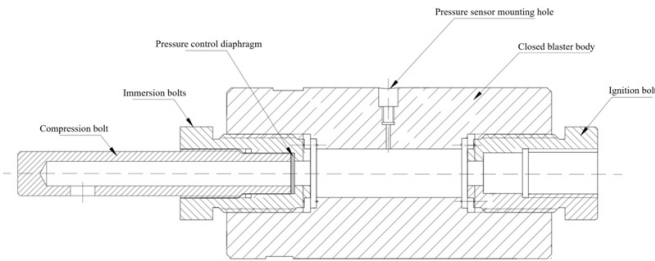


Figure 2. Closed explosive device schematic diagram.

The actual airtight explosive device is shown in Fig. 3. In the actual test process, the ignition device detonates the small detonator in the closed detonator by means of electric initiation, and the detonator and the propellant are stuck together to detonate the propellant, thus producing high-temperature and high-pressure gas. When the pressure in the detonator reaches the rated value, the high-temperature gas breaks through the pressure control diaphragm and it is guided by the guide tube and finally acts on the heat flux density sensor sensitive mem-

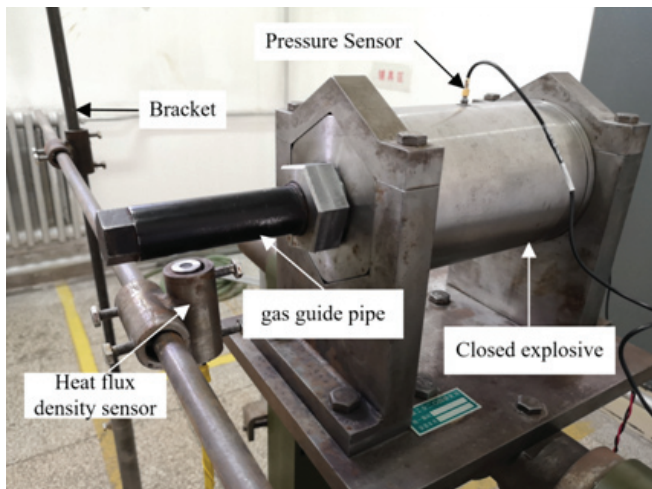


Figure 3. Closed explosive device physical map.

brane. The temperature of the heat flux density sensor thermal element is increased, and the voltage signal is collected by the output data collector. The pressure sensor is installed on the mounting hole of the explosive device body to test the pressure change curve in the explosive device.

### 2.3 Heat Flux Density Sensor

The heat flux density sensor is a contact heat flux density sensor based on infrared temperature measurement technology. The sensor structure schematic diagram is shown in Fig. 4.

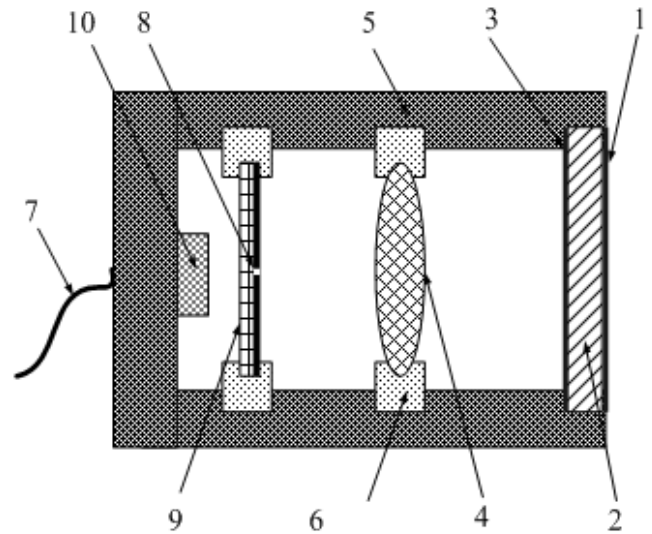


Figure 4. Heat flux density sensor structure schematic diagram.

Among them, 1 is a coating with high absorption ratio, the material is black nickel, and the coating thickness is  $10 \mu\text{m}$ ; 2 is a thin-walled structure, made of copper, with a thickness of  $1\text{mm}$ ; 3 is a high emissivity coating, the material is carbon black, and the coating thickness is  $8 \mu\text{m}$ ; 4 is an infrared optical lens. In order to make the lens have a high transmittance in the middle and far infrared regions, the lens material is zinc selenide, the diameter of the lens is designed to be  $0.025 \text{ m}$ , and the focal length is  $5\text{mm}$ ; 5 is the shell; 6 is the lens clamping device; 7 is the output wire; 8 is a light transmission hole; 9 is the filter; 10 is an optical electric conversion module, and the module model is HMS Z11 infrared thermopile.

Under the effect of environmental heat flow density, the coating with high absorption ratio receives the near-infrared energy radiated by the explosion fireball, and the absorptivity of the carbon black surface is about 0.8, and changes steadily in the spectral range; The high emissivity coating material can transfer the energy absorbed by the front end face to the optical lens with the minimum attenuation amplitude. Radiated infrared optical signal is focused by the lens and reaches the light-transmitting hole. The electrical conversion module accepts the infrared light signal emitted by the rear wall of the thermal element and converts it into a voltage signal, and then measures the rear wall temperature. Finally, the incident heat flux density is obtained by combining the rear wall temperature of the thermal element and the sensor mathematical model. The sensor is self-developed by Nanjing University of Science and Technology. The physical image of the sensor is shown in Fig.

5. The main technical indicators of the sensor are shown in the following Table 2.

**Table 2. Technical indexes of heat flow density sensor**

Technical indicators	Indicator parameters
Response time	$\leq 3$ ms
Test range	0-20 MW/m <sup>2</sup>
Maximum heating capacity	$\geq 20$ M J/m <sup>2</sup>
Measurement uncertainty	Better than 3 % (k=2)
Repeatability	Better than 5 % FS



**Figure 5. Heat flux density sensor physical map.**

### 3. DATA PROCESSING AND ANALYSIS

#### 3.1 Mathematical model of heat flux density sensor

The heat flux density sensor mathematical model can be expressed as:<sup>16</sup>

$$q(t) = \rho c l \frac{dT}{dt} \quad (1)$$

Among them:  $\rho$  is the density of the sensitive element, the unit is kg/m<sup>3</sup>;  $c$  is the specific heat capacity, the unit is J/(kgK);  $l$  is the thickness, the unit is m;  $T$  is the temperature, the unit is °C;  $t$  is the time, the unit is s.

The sensor used in this test first detects the temperature rise curve of the rear wall of the thermal element through an infrared thermopile, and then calculates the heat flux density according to the density, specific heat capacity and thickness of the sensitive element. The sensitive element of the heat flux density sensor used in the experiment is copper with a thickness of 0.001 m, and in the process of calculating the heat flux density, it is assumed that the density of the sensitive element is 8430 kg/m<sup>3</sup> and the specific heat capacity is 385 J/(kg°C).<sup>17-18</sup>

In the actual test process, due to the mounting bracket vibration, the impact of the propellant combustion process, electromagnetic interference and other factors, the test data has a large noise. If the above Eqn. (1) is directly used to calculate the test data, the accuracy of the calculation results will be greatly affected by the noise due to the existence of

interference noise in the test signal. Therefore, we first use the third-order polynomial to perform nonlinear adaptive fitting on the test data to obtain the overall change trend of the test data, and then calculate the heat flux density according to the fitting temperature rise curve combination formula (1), which reduces the impact of test noise on the calculation results to a certain extent.

#### 3.2 Test Results and Analysis

A total of three propellant deflagration were carried out in this test. After the test was completed, the heat flux density sensor data was extracted and processed, the three rounds ammunition variation curve of the deflagration temperature with time was obtained as shown in Fig. 6. In Fig. 6, the abscissa represents the acquisition time of the data acquisition system, denoted by  $t$ , and the unit is second (s). The ordinate represents the temperature change value during the ammunition deflagration, denoted by  $\Delta T$ , in degrees celsius (°C).

Analysis of the temperature time-history curve in Fig. 6 shows that:

1. In the deflagration process, the ammunition has a rapid heating process, and the temperature rises very rapidly. As shown in Fig. 6(a), the temperature of the thermal element rear wall rises rapidly between 30.072-30.082 s, as shown in Fig. 6(b) the temperature of the medium thermal element rear wall rises rapidly between 3.253-3.265 s, and the temperature of the thermal element rear wall in Fig. 6(c) rises rapidly between 2.522-2.532 s; and the high temperature duration is very short.
2. The variation laws of the three temperature curves have strong consistency, and it can be divided into three parts. The first part is from the beginning of the temperature rise to the first temperature peak, the second part is the temperature rising for the first time and then starts to rise to the second peak, and the third part is the temperature rising steadily. Since there are two peaks in the temperature curve, which does not conform to the theoretical propagation law of the deflagration thermal effect, the reason for this problem is analysed to protect the heat flux density sensor, the structure of the airtight explosive device is improved, so that the outlet of the high-temperature gas is not in the guide tube. On the axial direction of the guide tube, and below the guide tube, it is 90° from the axial direction of the guide tube, so that the high-temperature gas is turned outward in the process of spreading out compared to the original, so that the temperature curve appears a second wave peak.
3. During the whole test process, the temperature of the thermal element continued to rise, but the temperature rise rate showed a trend of increasing and then decreasing. This is because the temperature rise of the thermal element is mainly affected by two aspects, one is the temperature rise caused by the shock wave compressed air wave front; the other is the temperature rise caused by the diffusion of high temperature combustion products. At the beginning of the test, under the combined action of two factors, the thermal element temperature increased rapidly, and the thermal element temperature

rose rapidly at this stage; after that, due to the shock wave pressure attenuation, the temperature rise of the thermal element was only affected by the diffusion of high-temperature combustion products, so the temperature rise rate gradually decreases. Through the trend analysis of the above temperature curve, the polynomial fitting method is used to solve its functional relationship. The fitting result shows that the above temperature curve satisfies the cubic equation, and the fitting effect is shown in Fig. 7.

The cubic function relations obtained by fitting the above three curves are shown in formulae (2), (3) and (4).

$$\Delta T = -6.48 \times 10^7 \times t^3 + 5.85 \times 10^9 \times t^2 - 1.76 \times 10^{11} \times t + 1.76 \times 10^{12} \quad (2)$$

$$\Delta T = -1.40 \times 10^7 \times t^3 + 1.36 \times 10^8 \times t^2 - 4.45 \times 10^8 \times t + 4.83 \times 10^8 \quad (3)$$

$$\Delta T = -1.50 \times 10^7 \times t^3 + 1.13 \times 10^8 \times t^2 - 2.85 \times 10^8 \times t + 2.39 \times 10^8 \quad (4)$$

To verify the fitting accuracy of Eqns. (2)-(4) to the measured data, the calculated value of the above fitting function relationship is compared with the measured value, and the absolute error histogram of Eqns. (2)-(4) and the measured temperature value is shown in the following Fig. 8.

From the absolute error histogram of the calculated value and the measured value of the above function relationship, it can be seen that the formula (2)-(4) has a good interpretation ability for the existing measured data, the function relationship fits with high accuracy, meets the needs of actual engineering testing, and can be used to numerically quantify the change of temperature curve during the deflagration of the propellant.

According to the cubic function fitting relationship obtained by the above fitting, the heat flow density curve under the three deflagration tests is calculated, as shown in Fig. 9.

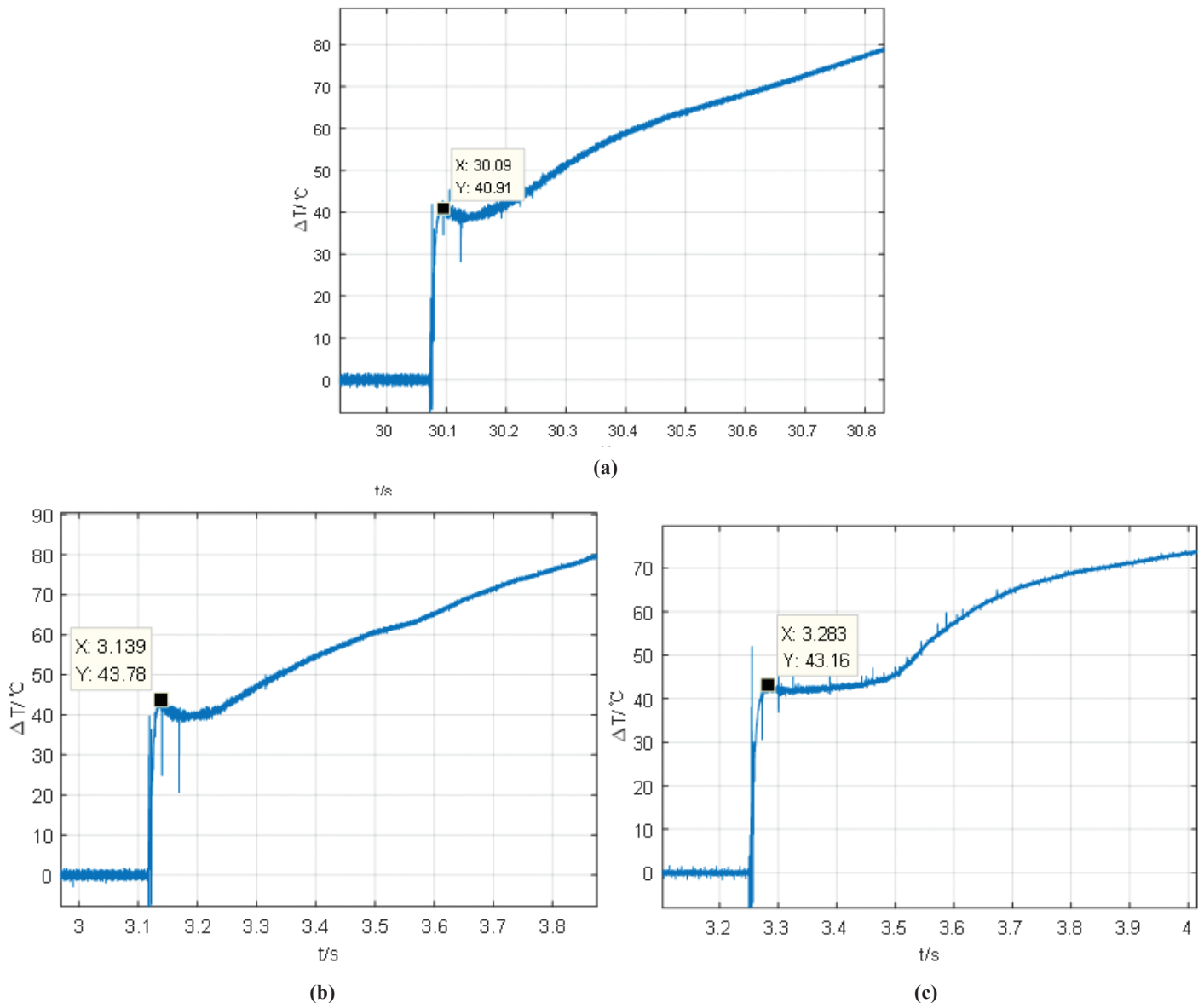
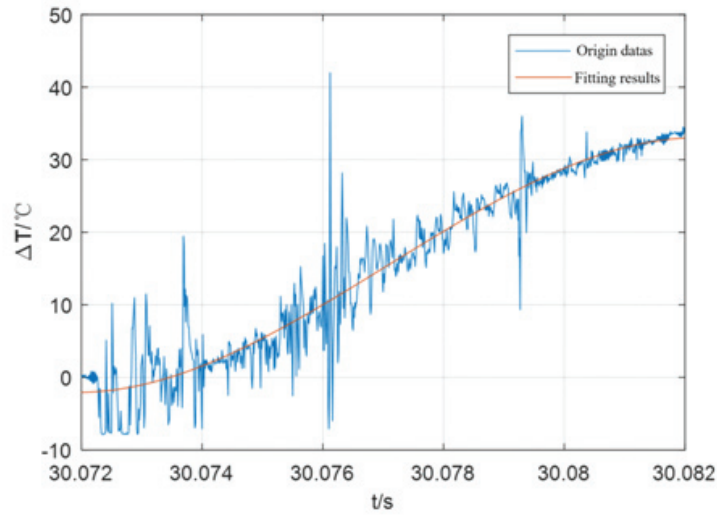
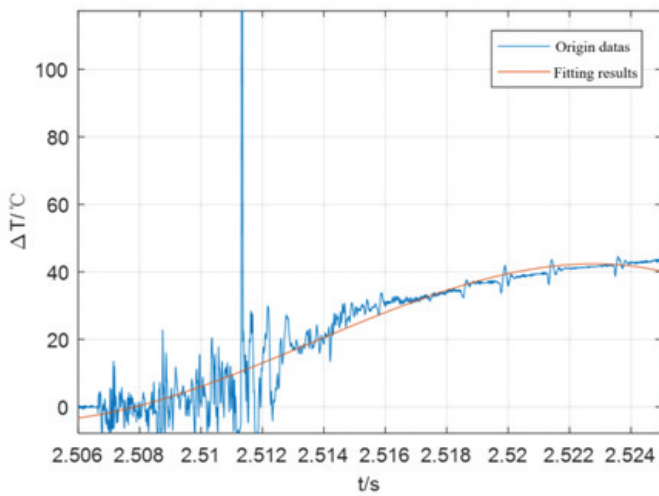


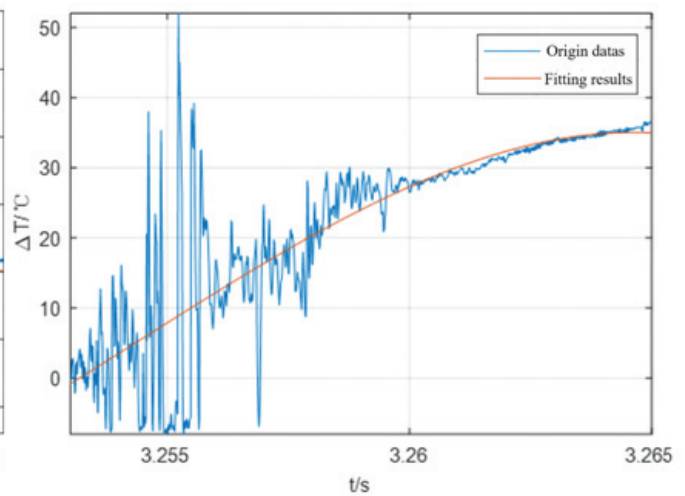
Figure 6. Deflagration temperature time-history curve of three rounds of ammunition: (a) First round of ammunition, (b) Second round of ammunition, and (c) Third round of ammunition.



(a)

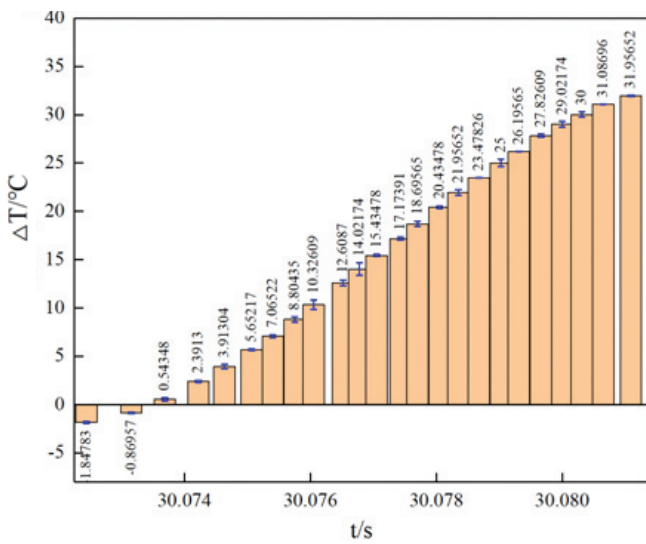


(b)

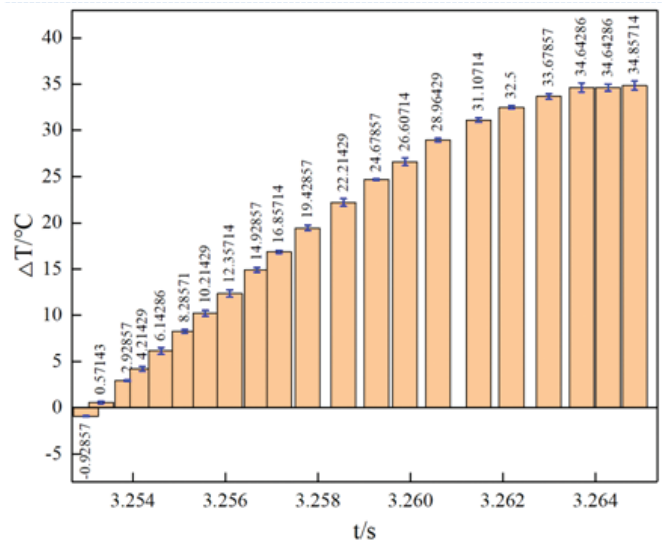


(c)

Figure 7. Cubic function fitting effect diagram of temperature curve: (a) First round of ammunition, (b) Second round of ammunition, and (c) Third round of ammunition.

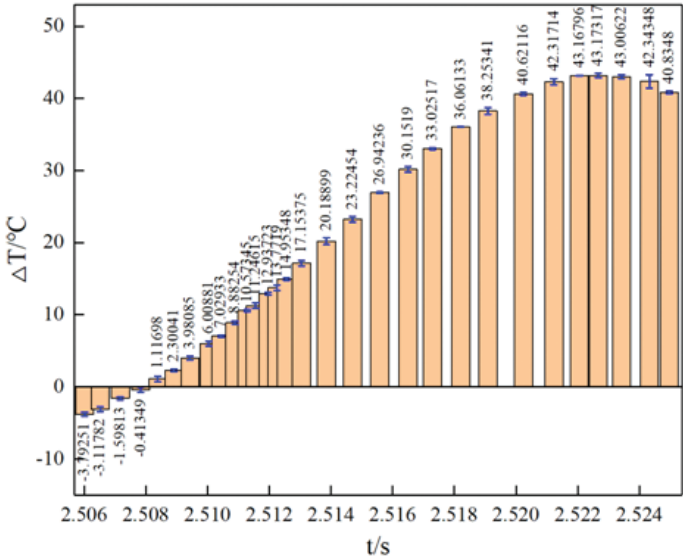


(a)



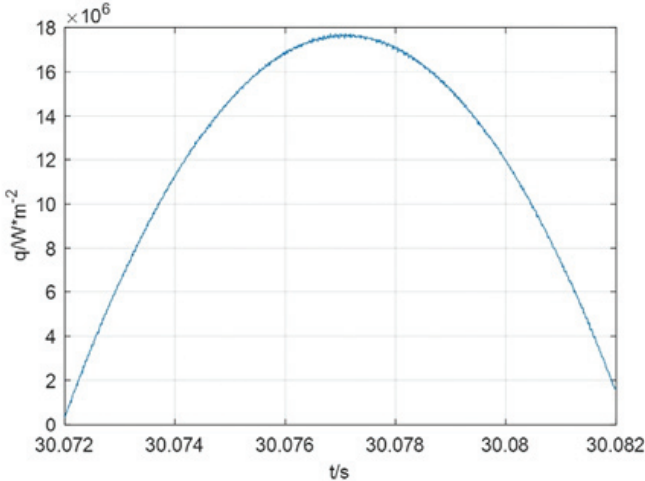
(b)

Figure 8(a) & (b). Absolute error histogram of calculated value and measured value: (a) Equation 2 Absolute error histogram of calculated value and measured value, (b) Equation 3 Absolute error histogram of calculated value and measured value.

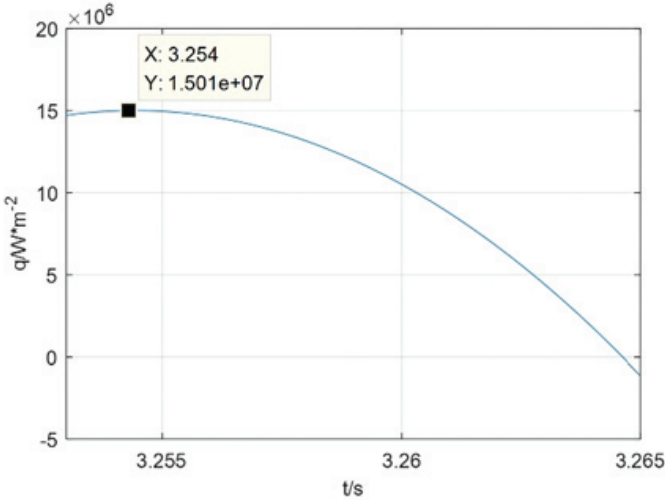


(c)

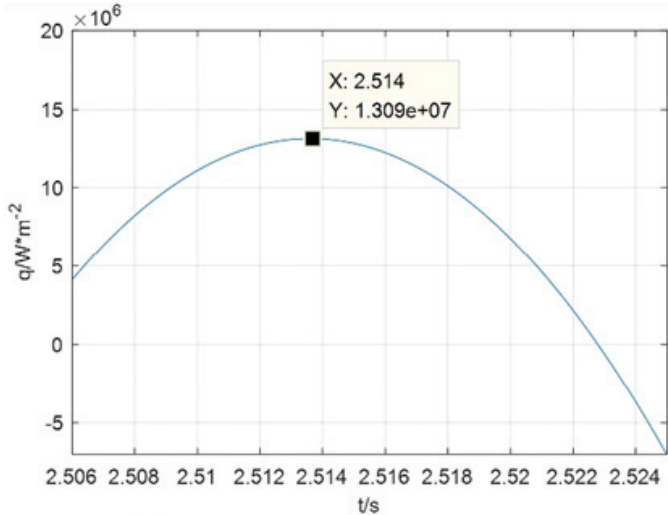
Figure 8(c). Absolute error histogram of calculated value and measured value: Equation 4 Absolute error histogram of calculated value and measured value.



(a)



(b)



(c)

Figure 9. Three rounds of ammunition heat flux curve: (a) First round of ammunition, (b) Second round of ammunition, and (c) Third round of ammunition.

From the curve in Fig. 9 above, it can be concluded that the heat flux density generated by the deflagration of the three propellants is different, the maximum value of the first heat flux density is 17.68 MW/m<sup>2</sup>, the maximum value of the second heat flux density is 15.01MW/m<sup>2</sup>, and the maximum value of the third heat flux density is 13.09 MW/m<sup>2</sup>. Because the environment of each test cannot be absolutely consistent, such as the temperature of the closed explosive device body, the charging parameters of the test propellant column, etc. the heat flux generated by deignition of the same propellant will have a certain difference, but the difference is not large, and the heat flux curve overall change trend is relatively consistent, indicating that the test method is correct.

#### 4. CONCLUSION

In this study, the thermal shock characteristics of 5/7 single base propellant deignition were studied by using an improved closed explosive. The heat flux data and curves of the three tests were obtained by data acquisition system. The analysis results show that the temperature of the 5/7 single-base propellant rises rapidly during the deflagration process, and the maximum heat flux value is 17.68 MW/m<sup>2</sup>; the temperature curve of the three tests is affected by the structure of the closed detonator device to a certain extent, resulting in an inflection point during the rise in the temperature curve, but the three curves are in good agreement in trend. It shows that the improved closed explosive device can be used in the thermal shock characteristic test of propellant, and the improved device can avoid the damage of the sensor caused by the fragments directly hitting the sensor sensitive surface after the pressure relief film is broken, reducing the damage rate of the heat flow sensor during the test.

#### ACKNOWLEDGMENT

This work is supported by National Foundation Strengthening Program Key Research Project and National Equipment Program of China, project numbers 2021-JCJQ-ZD-360-11 and 14021001050206.

#### REFERENCES

1. Wang, L.X.; Dai, Y.; Wang, J.G. Experimental study on the effect of primer initial temperature on energy release characteristics. *J. of Ballistics*, 2022, **34**(2),106-110. doi:10.12115/j.issn.1004-499X(2022)02-0 16
2. Zong, S.J.; Yang, C.X.; Li, B.M. Wavelet analysis of pressure signal in plasma ignition airtight detonato. *J. of Artillery Launch and Control*, 2022, **43**(2), 75-80. doi:10.19323/j.issn.1673-6524.2022.02.01 3.
3. Huang, K.; Liu, D.Y. Experimental study on the relationship between the combustion velocity and temperature of a certain fracturing gunpowder. *Chinese J. of Ballistics*, 2020, **32**(2), 62-66. doi:10.12115/j.issn.1004-499X(2020)02-0 10.
4. Zhao, X.L.; Zhang, X.B. Erosion, combustion and flow characteristics of inner hole of tubular propellant. *Energ. Mater.*, 2019, **27**(3), 202-209. doi:10.11943/CJEM2018080.
5. Wang, J.J.; Huang, Y.S.; Ge, M.Z. Combustion performance of the exciter for flyer detonators. *Blasting Equip.*, 2017, **46**(1), 38-40+45. doi:10.3969/j.issn.1001-8352.2017.01.z00 8.
6. Ni, Y.J.; Xing, R.J.; Wan, G. Porous propellant plasma enhanced burning rate. *Explos. and Shock*, 2016, **36**(04), 56 2-567. doi:10.11883 /1001-1455( 2016) 04-0562-06. doi:10.14077/j.issn.1007-7812.202012029.
7. Zhao, Y.H.; Xiao, Z.G.; Yan, W.R. Prediction of the internal ballistic performance of the launching charge based on the enclosed explosive device test. *J. of Propellant and Explos.*, 2020, **43**(1), 81 -84+89. doi:10.14077/j.issn.1007-7812.201901010.
8. Liang, X.A.; Nie, J.X.; Wang, S. Research on the output performance of Al/KClO<sub>4</sub> igniter in a closed explosive device. *J. of Ordnance Eng.*, 2017, **38**(8),1513-1519. doi:10.3969/j.issn.1000-1093.2017.08.008.
9. Ren, W.Y.; Pan, Y.T.; Cui, Y.H. Study on the pressure change of the closed explosive test process. *Mech. Eng. and Automat.*, 2013, **4**, 21-23.
10. Wang, Q.L.; Zhao, X.F.; Liu, S.W. A quantitative evaluation method for incremental combustion increasing of propellant based on the test of closed explosives. *J. of Fire and Explos.*, 2009, **32**(3), 71-74. doi:10.14077/j.issn.1007-7812.2009.03.01 9.
11. Jiang, D.d.; Xue, X.c. Internal ballistic characteristics of combustion propulsion process of packaged liquid propellant [J]. *J. of Military Eng.*, 2021, **42**(4), 755-763. doi:10.3969/j.issn.1000-1093.2021.04.009.
12. Sun, M.l.; Lu, L.; Liu, N. *et al.* Internal ballistic combustion stability of liquid propellant mortars [J]. *J. of Ordnance Industry*, 2020, **41**(11), 2145-2154. doi:10.3969/j.issn.1000-1093.2020.11.001.
13. Xiong, J.M.; Lu, X. Study on grain crushing model of counter sunk charge [J]. *J. of Weapon Equip. Eng.*, 2022, **43**(8), 140-145. doi:10.11809 /bqzbgcxb2022.08.022.
14. Feng, B.B.; Rui, X.T.; Chen, T. Influence of pressure loss of airtight explosive on initial dynamic activity ratio. *J. of Ballistics*, 2012, **24**(3), 6-9. doi:1004-499X (2012)03-0006-04.
15. Yang, C.X.; Jin, Y.; Li, H.Y. Experimental research on consistency of plasma ignition in airtight detonator. *J. of Ballistics*, 2015, **27**(3), 58-61.
16. Jiang, T. Design of a new heat flux sensor based on infrared detection [J]. *Foreign Electron. Meas. Technol.*, 2017, **36**(11), 38-42.
17. Zhang, J.F.; Su, J.J.; Ji, J.R. Development and application of heat capacity heat flux density sensor. *China Test*, 2018, **44**(10), 125 -129. doi:10.11857/j.issn.1674-5124.2018.10.0 21.
18. Zhou, L.L. Development of a new high temperature transient heat flux sensor based on thin film thermopile[J]. *Aerosp. Meas. Technol.*, 2018, **38**(6), 50-56. doi:10.12060/j.issn.1000-7202.2018.06.09.

## CONTRIBUTORS

**Dr Liangquan Wang** received his PhD from Nanjing University of Science and Technology. His current research interests include blast field damage measurement testing and evaluation.

He is responsible for the writing and revision of this manuscript.

**Dr Fei Shang** received his PhD from Jilin University. His current research direction includes special environmental

parameter testing technology and damage power testing and evaluation research. He is responsible for the overall review of this manuscript.

**Dr Deren Kong** received his PhD from Nanjing University of Science and Technology. His current research direction is the modern test measurement theory and application.

He is responsible for overall organization of this manuscript.